A signal-on electrochemical aptasensor based on silanized cellulose nanofibers for rapid point-of-use detection of ochratoxin A

Ahmed Y El-Moghazy, Noha Amaly, Georges Istamboulie, Nitin Nitin, Gang Sun

HHS Public Access

Author manuscript

Mikrochim Acta. Author manuscript; available in PMC 2021 September 01.

Published in final edited form as:

Mikrochim Acta. ; 187(9): 535. doi:10.1007/s00604-020-04509-y.

A signal-on electrochemical aptasensor based on silanized cellulose nanofibers for rapid point-of-use detection of Ochratoxin A

Ahmed Y. El-Moghazy[1,2], **Noha Amaly**[1,2], **Georges Istamboulie**[3], **Nitin Nitin**[1,4], **Gang Sun**[1]

[1]Department of Biological and Agricultural Engineering, University of California, Davis, CA 95616, USA.

[2]Polymeric Materials Research Department, Advanced Technology and New Materials Research Institute, City of Scientific Research and Technological Applications (SRTA-City), New Borg El-Arab City 21934, Alexandria, Egypt.

[3]Univ. Perpignan Via Domitia, Biocapteurs-Analyses-Environnement, 66860, Perpignan, France.

[4]Food Science and Technology, University of California, Davis, United States.

Abstract

An innovative ultrasensitive electrochemical aptamer-based-sensor was developed for Ochratoxin A (OTA) detection in cold brew coffee through revolutionary combination of nanofibers, electrochemical and aptamer technologies. The assembly of the aptasensor was based on the activation of silanized cellulose nanofibrous membranes as a supporting matrix for methylene blue (MB) redox probe labeled aptamer tethering. Cellulose nanofibrous membranes were regenerated by deacetylating electrospun cellulose acetate nanofibrous membranes with deacetylation efficacy of 97%, followed by silanization of the nanofiber surfaces by using 3-aminopropyl triethoxysilane (APTES). A replacement of conventionally casted membranes by the nanofibrous membranes increased the active surface area on the working electrode of a screen-printed three-electrode sensor by more than two times, consequently enhancing the fabricated aptasensor performance. The developed aptasensor demonstrated high sensitivity and specificity toward OTA in a range of 0.002-2 ng mL^{-1}, with a detection limit of 0.81 pg mL^{-1}. Moreover, the assembled aptamer-based-sensor successfully detected OTA in cold brew coffee samples directly without any pretreatment. The aptasensor exhibited good reusability and stability over storage time.

Keywords

Cellulose; Nanofibers; Aptamer; Ochratoxin A; Electrochemical aptasensor; Point-of-Use; Coffee

Introduction:

Coffee is with no doubt the most popular and growing consumed functional beverage over the world [1]. Drinking coffee is a part of many lifestyles and recognized with stimulatory and healthy effects owing to the wide range of bioactive components and antioxidants it contains [2-4]. Cold brew coffee is gaining a growing positive attention from the consumers around the world, where its US market raised by about 580% in the last five years and

gained $38 million in sales in 2017 alone [5]. While in 2018, the global size of the cold brew coffee market was valued by $339.7 million with expecting growth to reach $1.63 billion by 2025 [6].

However, coffee could contain unfavorable and harmful substances such as toxigenic fungi and their secondary metabolites such as ochratoxin A (OTA). OTA has been detected in different countries before and after the roasting of coffee beans, where the roasting process could not significantly reduce OTA content in coffee [7-9]. OTA is one of the most frequently found, harmful and poisonous contaminant among all mycotoxins [10, 11]. Moreover, the presence of such chemicals in coffee may have a negative impact economically on the producing nations.

This acute toxic present in the coffee samples in the part per billion concentrations. The European Commission imposed limits for OTA of 5 ppb for roasted coffee beans, ground roasted coffee and raw cereal grains, and 3 ppb in processed cereal foods [12, 13]. Based on recently reported existence of OTA in coffee beans in international markets, the average contents of OTA were found between <0.1-4.2 ppb [7-9, 14].

The detection and determination of such low level of toxins in coffee products are only carried out by using ultrasensitive and specific analytical instruments and methods. Typical analytical methods for OTA detection in foodstuffs are chromatography analytical methods and immunosensing assay systems [15, 16]. Despite of the high sensitivity and selectivity, the chromatography analytical methods have many drawbacks hindering the *in-situ* monitoring of OTA in coffee, such as requirement of highly trained professionals, use of costly equipment, lengthy sample preparation and testing times. Moreover, the sensitivity of ELISA systems is relatively low. In addition, these immunoassays are using antibodies and enzymes which suffer from disadvantages such as the high cost of antibody/enzyme production and ease denaturation of antibody/enzyme during storage [17].

The electrochemical biosensing technology has been introduced as an attractive, advantageous, and promising alternative for the traditional methods[18]. Aptamers are a new class of molecules, serving as innovative sensing tool suitable to detect different biological targets. The aptamers are single stranded oligonucleotides (DNA or RNA) and have the ability similar as an antibody to bind the target. These aptamers have several advantages comparing to the conventional antibodies, including less expensive and easier to produce, and more stable for reuses. Moreover, the aptamers can be tagged easily with different kinds of labels, consequently increasing the suitability for other detection methods [19]. Therefore, the aptamers are considered as an appropriate surrogate to the different biomolecules in the fabrication of various sensitive, miniaturized, and selective sensing systems. The electrochemical aptasensors are gaining a growing attention, and several efforts have been reported for detection of the different mycotoxins by coupling the electrochemical and aptamer technologies [20-25].

Cellulose is the most popular natural polymer on our planet and is considered as the key material to unlock the gate toward a forthcoming sustainable society because of its attractive properties such as renewability, hydrophilicity, biocompatibility, biodegradability,

availability, and thermal stability [26]. Nowadays, cellulose has received growing attention in a wide scope of applications, for instance, sensors, coatings, packaging, drug delivery, and flexible electronic systems [27-31].

Electrospinning process is a straightforward and cost-effective method for producing microporous nanofibrous membranes, which can serve as a unique matrix with desired flexibility, huge surface area, as well as high porous structure. The applications of the membranes in biosensors can provide a very large sensing surface area and easy access for contaminants to the sensing sites. Additionally, the microporous nanofibrous structure offers the advantage of desirable microenvironment and facilitate the movement of the electrons between the active sites and the electrode [32-34]. Cellulose nanofibers (CNFs) show promising results in immobilization of biomolecules. Nevertheless, the high crystallinity of CNFs acts as a barrier in the directly electrospinning of the cellulose to nanofibrous membranes [35]. As an alternative, cellulose acetate can be electrospun into nanofibrous membranes, which can be subsequently deacetylated to result in cellulose nanofibrous membranes [36, 37].

In this work, we integrate advantages of different technologies in development of an ultrasensitive electrochemical sensing system, including functionalized cellulose nanofibrous membranes as a supporting matrix and redox probe tagged aptamer as a signaling label. The proposed highly-sensitive aptasensor was assembled by covalently attaching methylene blue electroactive probe tagged anti-OTA aptamers onto the surface of silanized cellulose nanofibrous membranes which was incorporated on a disposable screen-printed carbon electrode (SPCE). The assembled apasensor was used for OTA detection using Differential pulse voltammetry (DPV) in the cold brew coffee.

2. Materials and methods:

2.1. Reagents

Cellulose acetate (CA; white powder; Mw = 30,000 Da), N, N-dimethylacetamide (DMAc), (3-aminopropyl)triethoxysilane (APTES), Ochratoxin B, Aflatoxin B1, Aflatoxin G1 were purchased from Sigma (St. Louis, MO) and used as received. Ochratoxin A (from *Aspergillus ochraceous*) was purchased from Enzo Life Sciences (Farmingdale, NY, USA). N-Ethyl-N′-(3- dimethyl aminopropyl) carbodiimide hydrochloride (EDC), N-hydroxyl succinimide (NHS), disodium hydrogen phosphate (Na_2HPO_4), and monosodium orthophosphate (NaH_2PO_4) were supplied by Acros Chemical (Pittsburgh, PA, USA). Graphite (Electrodag 423SS) and silver/silver chloride (Electrodag 418SS) inks were obtained from Acheson (Plymouth, UK).

The anti-OTA aptamer tagged with redox probe methylene blue was purchased from Biosearch Technologies (Novato, CA, USA). The aptamer sequences are shown below as that its 5’ end was modified with $COOH^-$ and 3′ end was methylene blue tagged. 5′-GAT CGG GTG TGG GTG GCG TAA AGG GAG CAT CGG ACA-3′. This aptamer has an affinity K_d of 49 nM toward OTA [38]. Aptamer solutions were prepared in phosphate buffer saline (PBS) at pH 7.4.

2.2. Cellulose nanofibrous membranes production and functionalization:

2.2.1. Regenerated cellulose nanofibrous membranes production—The cellulose acetate nanofibrous membranes *via* electrospinning were obtained by using of a DXES-1 spinning equipment according to Amaly *et al.* [31]. Cellulose acetate NFMs were deacetylated to generate cellulose nanofibrous membranes (Cel NFMs). The deacetylation process was carried out in 0.05 M NaOH in 1:1 EtOH / water solutions at the room temperature for 48 hr to hydrolyze the acetate groups and to produce Cel NFMs. After subsequent rinsing with ultrapure water, the obtained Cel NFMs were dried at 80 °C for 12 h in a vacuum oven. The acetyl % of the generated cellulose membranes was measured by immersing a membrane sample in 20 mL of 0.05 N NaOH in 50% ethanol for 12 h at ambient temperature and followed by titrating of excess alkali with 0.05 N HCl using a pH meter. The percentage of acetyl % in cellulose was calculated according to equation (1) [39]:

$$\text{Acetyl } \% = (V_B \,.\, C_B - V_A \,.\, C_A)\, 4.3 \,/\, W \quad (1)$$

Where W is the sample weight, V_B and C_B are the volume and concentration of NaOH solution, and V_A and C_A are the volume and concentration of HCl solution, respectively.

2.2.2. Cel NFMs functionalization with silane coupling agent—The functionalization step with APTES was performed by immersing the Cel NFMs in APTES/ anhydrous toluene solution at concentration of 10 % (v/v) under vigorous stirring at 80 °C for 60 min. Following the functionalization, the Cel NFMs were then rinsed with toluene and ethanol to remove any APTES residual, dried at 80 °C, and finally designated as Cel–NH_2 NFMs.

2.3. Immobilization of methylene blue tagged Aptamer onto Cel-NH_2 NFMs

A 4 mm Cel NFM disc with 0.05 mm thickness was laminated on the working electrode of the SPCE using a conductive paste to fabricate Cel NFM/SPCE, and similarly Cel casted membranes were used for in parallel preparing of Cel CM/SPCE. The aptamer marked with the methylene blue (MB) redox probe and carboxylic group on 3' and 5' ends, respectively. Prior to the immobilization, the 5′ end of the aptamer was activated by EDC/NHS mixture at a concentration of 100/25 mM for 1 hr. A 20 μL of EDC/NHS preactivated aptamer solution at concentration of 1.5 μmol/L was dropped on the Cel-NH_2 NFM/SPCE and incubated for one hour in humid atmosphere condition. Subsequently, the resultant electrode (Apt/Cel NFM/ SPCE) was washed to remove any unbounded aptamer by using PBS several times, followed by blocking the remaining active groups with 100 μL of 2% ethanolamine (EA) at room temperature for 1 hr, then rinsed again with PBS and stored at 4°C to use.

The functional performance of the assembled sensor-based-aptamer was investigated by dropping of 100 μL of OTA solution at different concentrations on the surface of the aptasensor for 30 min incubation time. Prior to the electrochemical measurements, any unreacted OTA was removed by washing.

2.4. Electrochemical measurements

The screen-printed electrodes were fabricated based on the three-electrode system as described previously [40]. The electrochemical characterizations for the assembled sensor-based-aptamer were performed by cyclic voltammetry and Electrochemical impedance spectroscopy (EIS) in a 2.5 mM ferri/ferrocyanide ($[Fe(CN)_6]^{4-/3-}$) solution. The signal generation was based on the reduction of MB redox probe, which was recorded by Differential pulse voltammetry (DPV) using the following parameters: 0.5 s interval time, 0.005 V step potential, 0 V standby potential, 0.10005 V modulation amplitude, applied potential range of −200 – −700 mV *vs* Ag/AgCl. The electrochemical measurements were conducted at least in triplicates using a 263A potentiostat/galvanostat equipped with a frequency response detector (FRD100) (Princeton Applied Research Co., Oak Ridge, TN, USA).

2.5. Real sample analysis

The assembled aptasensor applicability was investigated for OTA detection in cold brew coffee, the coffee samples were purchased from a local market. The absence of OTA firstly was confirmed using HPLC before spiking the cold brew coffee samples with various OTA concentrations in the range of 0.01 - 1 ng mL^{-1}. The aptasensor was used for directly analyses of the spiked samples without any pretreatment, using DPV at applied potential range of −200 – −700 mV *vs* Ag/AgCl.

3. Results and discussion

3.1. Sensing mechanism of the proposed OTA aptasensor

The OTA detection strategy using the designed aptasensor relied on target-initiated structure-changing of the attached redox probe labeled aptamer. Without OTA, the immobilized aptamer is kept in the unfolded form, and the methylene blue redox probe is relatively farther to the surface of the electrode. With the binding of OTA onto the aptamer, the aptamer structure is switched to G-quadruplex form, and this conformational change results in reduced distance between the electroactive probe and the electrode surface. As a result, the methylene blue probe comes close to the electrode surface, triggering increasing electrochemical signals on the redox probe.

A schematic diagram of the assembling process and sensing mechanism of the OTA aptasensor is illustrated in Scheme 1.

3.2. Physico-Chemical characterizations of the produced Cel NFMs

Cellulose nanofibrous membranes were first fabricated *via* a regeneration method from cellulose acetate nanofibers (Figure 1A). Fourier-transform infrared spectroscopy (FT-IR) was employed to confirm the successful conversion of acetate group of cellulose acetate to hydroxyl groups of cellulose. FT-IR spectra of the cellulose acetate NFMs and Cel NFM were collected with a Nicolet 6700 spectrometer.

Figure 1B presents the FT-IR spectra of the Cel NFM (curve b) and the pristine cellulose acetate NFM (curve a). As can be seen in the Figure 1B, a new characteristic peak appeared

at around 3450 cm^{-1} belonged to the stretching vibration of -OH, and the peak around 1750 cm^{-1} assigned to C=O of the ester of cellulose acetate disappeared after the conversion process, indicating successful conversion of acetate to hydroxyl groups.

SEM images of electrospun cellulose acetate NFMs in Figure 1 C and D demonstrated that the cellulose acetate nanofibers were aligned and assembled with average diameter of 290 nm as a non-woven fabric. The cellulose acetate nanofibers ester groups were converted through the deacetylation process to hydroxyl groups, the Cel NFMs still retained the morphology and similar average diameter (Figure 1 E and F).

Cellulose acetate concentrations (5, 10, 15 and 20 %) in electrospinning process affected nanofiber diameters and morphologies, which was studied to obtain the finest and uniform NFM with high surface areas. It is a key step to ensure the most important advantageous of microporous and nanofibrous structures with desired fast access to target molecules. As presented in Fig. S1, the nanofiber diameter increased by increasing cellulose acetate concentration, which could be due to increase chain entanglements at a higher concentration, as a result to the high resistance of the solution to stretching with rising the solution concentration [41]. Balancing the needs of small diameter, morphology of the membranes, and easy production, membranes produced from 10 % cellulose acetate solution was employed in the fabrications of the biosensors.

Deacetylation degree of the regenerated cellulose is a factor affecting the activation process of cellulose and subsequently efficiency of aptamer immobilization. The maximum deacetylation and removal of ester groups on the regenerated cellulose were achieved in aqueous as well as alcoholic NaOH solutions. The deacetylation % of CA in alcoholic NaOH solution was 85 % where in NaOH aqueous solution 97%, consistent with FTIR results (Fig. S2). The ester peak intensity changes at 1700 cm^{-1} indicate the conversion of cellulose acetate under both aqueous and ethanolic hydrolyses. Hydrolysis time could impact completeness of deacetylation, prolonged deacetylation process of 48 hours could reach maximum 97 % of removal of the ester groups (Fig. S3).

3.3. Activation of Cel NFMs surface

Silanization is a recognized and efficient process to activate the surfaces of cellulose for biomolecular immobilization in the development of biological platforms or microfluidic devices for cell and tissue engineering applications. The process provides simplicity and efficiency of establishing covalent connections between electrode surfaces and the biomolecules [42-44]. Herein, the functionalization of Cel NFMs with APTES works as an active spacer arm to afford the desired amine functional groups for immobilization of the MB labeled aptamer by reacting with its 5’-terminus end carboxylic group. Furthermore, it is necessary to keep the redox probe in a long distance from the surface of the electrode to reduce the background current generated from the unfolded aptamer in absence of the target, and consequently, improving the sensitivity of the assembled sensing system.

Ninhydrin color test, a common colorimetric indication of primary or secondary amine existence in materials, was utilized to indicate successful modification of the surface of the Cel NFMs by APTES, as the siloxane peak could not be accurately characterized by FTIR

due to an overlap with the stretching region of the acetal bonds of the Cel NFMs [45]. Ninhydrin test was conducted following a procedure reported by Qi and his colleagues [46]. According to the mechanism shown in Fig. 2a, by incubating the Cel-NH_2 NFMs with ninhydrin in ethanol, the light-yellow color of the ninhydrin solution turned to dark purple (Fig. 2b). This sharp color change reveals that APTES molecules were loaded on the cellulose chains.

Furthermore, EDX analysis was used to confirm the successful silanization of Cel NFMs hydroxyl group with the silane coupling agent. In the spectrum (Fig. 2c), the peaks of the carbon and oxygen were appeared. After the activation of the Cel NFM with APTES, Si peak was observed (Fig. 2d). This observation proved that chemical activation of the Cel NFMs by APTES was achieved.

The optimization of the silanization process was carried out by the Ninhydrin test as well. As shown in Fig. S4a, with rising APTES concentration the color intensity increased and reached at a maximum with APTES at 10 % (v/v). Similarly, increasing the activation time led to increase of the purple color intensity which plateaued at the activation time over 60 min (Fig. S4b).

The abovementioned results agreed well with the wetting properties of the different nanofibrous membranes. Hydrophobic/hydrophilic nature of the different surfaces was investigated by measuring contact angles of water droplets on the membranes to confirm the deacetylated then the silanization of the cellulose acetate NFMs and the Cel NFMs, respectively. The hydrolysis process of the cellulose acetate NFMs to the Cel NFMs led to decrease in the contact angle from 85° to immediately wet due to conversion of acetate groups of the cellulose acetate NFMs to hydroxyl groups in cellulose, increasing the hydrophilicity of the membranes. The water drop contact angle on the surface of the Cel NFMs was not measurable (Fig. S4c) since the water droplet is quickly absorbed onto the material surface. However, as expected, with the surface modification of the cellulose hydroxyl groups by the silane coupling agent, the membranes exhibit a hydrophobic surface with a contact angle of 52°. Thereby, this could serve as a further proof to the successful grafting of APTES molecules on the Cel NFMs surfaces.

3.4. Electrochemical characterization

The impact of the nanofibrous membranes to the immobilization matrix of the aptasensor was investigated by using screen-printed electrodes modified with Cel casted membranes (Cel CM/SPCE) and Cel nanofibrous membranes (Cel NFM/SPCE), respectively.

The effective surface area of the different modified electrodes was calculated according to Randles-Sevcik equation [47].

$$i_p = 2.69 \times 10^5 \, An^{3/2} D^{1/2} C v^{1/2} \quad [2]$$

where A is effective area of an electrode, n is electrons transferred number, D is the diffusion coefficient, C is $K_3Fe(CN)^6$ solution concentration while v is the scan rate. After achieving a linear correlation from plotting the peak current versus the square root of scan rate (Fig. 3A

inset) and according to the above equation, the effective surface areas of Cel CM/SPCE and Cel NFM/SPCE were found to be 9 and 25 mm^2, respectively (Fig. 3A). The higher electroactive surface area of the Cel NFM/SPCE in comparison with the Cel CM/SPCE is due to the unique microporous structure of the nanofibrous membranes that can facilitate easy access of analytes toward the surface of the electrode and accelerate the electron moving between the analyte and the electrode surface, making this unique material introduced as an ideal matrix for fabricating highly sensitive sensing systems.

EIS is a suitable tool for studying the surface features of the different modified electrodes through the assembling and the dynamic performances of electrochemical processes [48]. Herein, the EIS was used to prove the aptasensor fabrication steps. The impedance spectra contain two parts: the first portion at the higher frequencies is a semicircle that reveals the electron-transfer-resistance (R_{et}) of the electrode surface, while the second part at the lower frequencies is a linear portion which presents the diffusion-limited process [49].

The regenerated Cel NFMs were used as a tethering matrix for fabricating the aptasensor. Fig 3B confirmed the successful assembly of the sensor by showing the semicircle portion of the different electrodes and the electron transfer resistances, the unmodified SPCE reveals a very low resistance value (curve a). As shown in curve (b), the lamination of the Cel NFMs onto the SPCE surface led to an increase in the semicircle domain, due to hindrance of the nanofibrous membrane to the electron movement between the electrolyte solution and the electrode surface. Additional increase in the R_{et} was achieved after the silanization of the Cel NFM (curve c). The immobilization of the aptamer onto the Cel-NH_2 NFM (Apt/Cel NFM/SPCE) prompted an expansion in the resistance as can be seen in curve (d), and it could be attributed to the attached aptamer hindered the electron transfer and the repulsion between the negatively charged redox solution and the negative phosphate backbone of the aptamers. In the same vein, the blockage of the remaining amine groups by ethyleneamine (EA) in the membrane (EA/Apt/Cel NFM/ SPCE) induced increase in the R_{et} (curve e), an evidence of the effective blocking step. With the existence of OTA in the system (OTA/EA/Apt/Cel NFM/SPCE) (curve (f)), the binding of the OTA molecules with the anchored aptamer led to deterrence of the electron transfer and consequently further increase in the semicircle diameter, probably owing to conformational changes of the attached aptamer to G-quadruplex form after binding with OTA molecules. Also, this increase of the R_{et} could be caused by the presence of the carboxylic groups and phenolic moieties of OTA molecules. The above-mentioned results confirmed the successful completion of every steps of the sensor-based-aptamer fabrication process.

3.5. Optimization of experimental parameters

3.5.1. Aptamer concentration—Aptamer concentration is another key parameter for the sensitivity of the biosensor as high concentrations of the aptamer may influence the detection limit owing to the self-complementary between the neighboring individual aptamers. Also, increase of the aptamer concentration leads to increase of both negative current from the unfolded state and costs of analysis [50].

As shown in Fig. S5A and S5B (curve a), the negative current increased with the increment of aptamer concentration from 0.25 to 3 μmol/L. In presence of 0.5 ng mL^{-1} OTA (Fig. S5B

curve b), with increase of the aptamer concentration from 0.25 μmol/L, the generated current obviously was increased to reach a maximum at the concentration of 2 μmol/L and then declined afterward. The reduction of the current could be caused by hindering effect of the additional immobilized aptamer onto the surface of the matrix to the transfer of the electrons toward the electrode surface. Thus, a concentration of 1.5 μmol/L was chosen for the further experiments as it provides the proper current signal with lowest background current (Fig. S5A (*inset*)).

3.5.2. Immobilization time—The required time for attaching the aptamer onto the silane coupling agent grafted Cel NFMs/SPCE was adjusted with the tethering time increased from 20 to 120 min. It can be seen in Fig. S5C that the peak current changed alone with the increase in the binding time of the aptamer on the surface of Cel-NH_2 NFMs from 20 min up to 60 min, resulting in an increase of the current signal, and then a plateau at the immobilization time over 60 min, indicating a saturation of the active sites on the nanofibrous matrix. Thus, the time of 60 min was used in the rest experiments for the aptamer attachment.

3.5.3. Aptamer-OTA reaction time—The optimization of the necessary time for incubating the aptasensor with the sample was carried out by exposing the assembled aptasensor with 0.5 ng mL^{-1} OTA for different durations. The signal responses obviously increased with the increase of the exposure time to reach to a plateau after the time of 30 min (Fig. S5D). Therefore, 30 min was chosen as a sufficient incubating time for the detection of the target OTA.

3.6. Analytical performance of the aptasensor

With optimizations of the different parameters, OTA was detected at different concentrations using the assembled aptasensor. As DPV responses illustrated in Fig. 4A, the obtained current increased with the rising OTA concentration. A proportional linear relation was achieved between the generated current and the logarithm of OTA concentration (Fig. 4B) in a range of 2 pg mL^{-1} to 2 ng mL^{-1} (R^2=0.9934), and the assembled aptasensor demonstrated a high sensitivity toward OTA with a limit of detection (LOD) at 0.81 pg mL^{-1} (LOD=$3S_d$ /b, where S_d is the blank standard deviation and b is the calibration plot slope.). Every experiment was carried out in triplicates.

Several researchers have reported developments of aptasensors for OTA detection, exhibiting superiority combining broad detection ranges and excellent LODs (Table 1). Most of the studies focused on enhancement of the sensitivity of the aptasenors by using conductive metals, which could increase the cost and background current, consequently decreasing the sensitivity of the sensor. Also, some of the impedimetric aptasensors [21, 22] require negative control samples, and others use a complementary aptamer sequences [21, 23, 24] in assisting DNA modified with MB, a more complicated method with increased analysis time. The aptasensor prepared in this work was developed based on a signal-on strategy with very low off-signal without using a control, consequently lowering risk of false positive. The use of the nanofibrous membranes could amplify the achieved current and enhance the performance of the sensor by about three time. Moreover, the aptasensor analysis time was

only 30 min, which could be attributed to the porous structure and high surface areas of the sensor matrix with facilitated access to the immobilized biorecognition elements and reduced diffusion limitation. These promising performances of the sensor in comparison with the other OTA aptasensor further demonstrated that the nanofibrous membranes are a desired matrix for the fabrication of highly sensitive biosensors.

3.7. Specificity, reusability, and stability of the assembled aptasensor

The specificity of the analytical tool toward the desired target is considered among of the most significant challenges, and the selectivity of the assembled nanofibrous-based-aptasensor was examined in the presence of ochratoxin B (OTB), aflatoxin B1 (AFB1), and aflatoxin G1 (AFG1). The responses of the aptasensor to AFB1, AFG1, OTB at the concentrations of 0.1 and 10 ng mL^{-1} and a mixture of them in presence of 0.1 ng mL^{-1} of OTA were measured. As shown in Fig. 5. There were no any significant cross-reactions or interferences observed for the OTA detection in coexisting of other common mycotoxins at the same concentration or with 100 folds higher than the OTA concentration in the sample. The achieved results confirm the high specificity of the fabricated sensor towards OTA detection.

The reusability of the nanofiber-based aptasensor was examined following a method as previously reported [52]. It was carried out by dropping 50 μL of a regenerating solution (methanol: regeneration buffer (10.0 mM TRIS, 1.0 mM EDTA, pH 9.0) (1:4 v/v) on the working electrode of the aptasensor for 30 sec, afterward extensively washing the sensor with deionized water. It was shown that the assembled nanofiber-based aptasensor is reusable after the simple regeneration approach. The regeneration step showed no significant impact on the aptasensor response in OTA detection for 6 cycles, and the developed aptasensor maintained about 86% of its initial activity after 9 assays.

Moreover, the stability of the proposed aptasensor over storage time is another crucial feature for a successful biosensing system. Therefore, the stability of the assembled sensor-based-aptamer was examined during a storage at 4 °C for 3 months, the current responses of the aptasensor nearly 92.3% of its initial value, demonstrating the assembled aptasensor has good storage stability.

3.8. Real samples analysis:

The feasibility of the developed sensors to real sample analysis without any tedious pretreatment is considered as the way to achieve the real goal as a point-of-use device. Herein, the fabricated sensor-based-aptamer was investigated to detect OTA in cold brew coffee samples directly without sample cleaning-up. Cold brew coffee samples were firstly analyzed using HPLC before spiking to confirm the absence of OTA, then were spiked with various OTA concentrations ranging from 0.01 to 1 ng mL^{-1}. The spiked samples were analyzed directly by the developed aptasensor, and each measurement was tested three times. As shown in Table S1, the recovery results demonstrate sensitive and quantitative OTA detection by the electrochemical aptasensor, appropriate to the directly within the real samples with recovery rates of 94.3% to 97.5% and a relative standard deviation (RSD%) of about 6.4%.

Although the promising advantages of rapid, portable, low-cost, specific, and sensitive characteristics, the aptasensor still has several key scientific limitations and challenges. The aptasensor is not compatible with the presence of ADNase in samples, pH conditions, and limited storage conditions of humidity and temperature. In addition, the screening of aptamers specific to mycotoxins is a complex and time-consuming process as until now only a few aptamers against mycotoxins such as OTA, AFB1 and fumonisin B1 have been successfully identified and applied. Therefore, the bottleneck problem on the development of mycotoxin aptasensors is how to identify and detect multiple mycotoxins using the limited variety of mycotoxin aptamers, especially for structurally similar mycotoxins [53].

Conclusion:

In this study, the developed nanofibers-based-aptasensor demonstrated the promising performance in fabricating highly sensitive electrochemical sensors. A rapid signal-on aptasensor was assembled using silanized cellulose nanofibrous membranes as supporting material for the immobilization of methylene blue electroactive probe tagged anti-OTA aptamers for OTA detection in the coffee beverages. The use of cellulose in nanofibers form as an immobilization matrix provides a high surface area with a microporous structure that can remarkably enhance the performance of the aptasensor comparable with and superior than the previous studies. These developed aptasensor could be applied in the limited resources sites, affording a rapid, specific, accurate and simple guarantee against contaminated staples.

Supplementary Material

Refer to Web version on PubMed Central for supplementary material.

Acknowledgment:

The research was partially supported by both USDA National Institute of Food and Agriculture (USDA-NIFA) program (Grant No. 2015-68003-23411) and National Institute of Environmental Health Sciences (NIEHS) (Grant No. 5P42ES004699).

References:

1. Bisht S, Sisodia S (2010) Coffea arabica: A wonder gift to medical science. J Nat Pharm 1:58 10.4103/2229-5119.73595
2. Meletis CD (2006) Coffee–Functional Food and Medicinal Herb. Altern Complement Ther 12:7–13. 10.1089/act.2006.12.7
3. Farah A, Donangelo CM (2006) Phenolic compounds in coffee. Brazilian J Plant Physiol 18:23–36. 10.1590/S1677-04202006000100003
4. Vignoli JA, Bassoli DG, Benassi MT (2011) Antioxidant activity, polyphenols, caffeine and melanoidins in soluble coffee: The influence of processing conditions and raw material. Food Chem 124:863–868. 10.1016/J.FOODCHEM.2010.07.008
5. Rao NZ, Fuller M (2018) Acidity and Antioxidant Activity of Cold Brew Coffee. Sci Rep 8:16030 10.1038/s41598-018-34392-w [PubMed: 30375458]
6. Grand View Research (2019) Cold Brew Coffee Market Size, Share, Industry Trends Report, 2025
7. Vanesa D, Ana P (2013) Occurrence of Ochratoxin A in coffee beans, ground roasted coffee and soluble coffee and method validation. Food Control 30:675–678. 10.1016/J.FOODCONT.2012.09.004

8. Galarce-Bustos O, Alvarado M, Vega M, Aranda M (2014) Occurrence of ochratoxin A in roasted and instant coffees in Chilean market. Food Control 46:102–107. 10.1016/J.FOODCONT.2014.05.014
9. Coronel MB, Marin S, Cano G, et al. (2011) Ochratoxin A in Spanish retail ground roasted coffee: Occurrence and assessment of the exposure in Catalonia. Food Control 22:414–419. 10.1016/J.FOODCONT.2010.09.012
10. Chrouda A, Sbartai A, Baraket A, et al. (2015) An aptasensor for ochratoxin A based on grafting of polyethylene glycol on a boron-doped diamond microcell. Anal Biochem 488:36–44. 10.1016/j.ab.2015.07.012 [PubMed: 26255699]
11. Rhouati A, Yang C, Hayat A, Marty J-L (2013) Aptamers: A Promising Tool for Ochratoxin A Detection in Food Analysis. Toxins (Basel) 5:1988–2008. 10.3390/toxins5111988 [PubMed: 24196457]
12. European Comission (2006) Comission Regulation (EU) no1881/2006
13. European Comission (2010) Comission Regulation (EU) no105/2010
14. Nakajima M, Tsubouchi H, Miyabe M, Ueno Y (1997) Survey of aflatoxin B1 and ochratoxin a in commercial green coffee beans by high-performance liquid chromatography linked with immunoaffinity chromatography. Food Agric Immunol 9:77–83. 10.1080/09540109709354938
15. Hayat A, Andreescu S, Marty J-L (2013) Design of PEG-aptamer two piece macromolecules as convenient and integrated sensing platform: Application to the label free detection of small size molecules. Biosens Bioelectron 45:168–173. 10.1016/J.BIOS.2013.01.059 [PubMed: 23500359]
16. Wu J, Chu H, Mei Z, et al. (2012) Ultrasensitive one-step rapid detection of ochratoxin A by the folding-based electrochemical aptasensor. Anal Chim Acta 753:27–31. 10.1016/J.ACA.2012.09.036 [PubMed: 23107133]
17. Shan H, Li X, Liu L, et al. (2020) Recent advances in nanocomposite-based electrochemical aptasensors for the detection of toxins. J Mater Chem B 8:5808–5825. 10.1039/d0tb00705f [PubMed: 32538399]
18. El-Moghazy AY, Soliman EA, Ibrahim HZ, et al. (2016) Ultra-sensitive biosensor based on genetically engineered acetylcholinesterase immobilized in poly (vinyl alcohol)/ Fe – Ni alloy nanocomposite for phosmet detection in olive oil. Food Chem 203:73–78. 10.1016/j.foodchem.2016.02.014 [PubMed: 26948591]
19. Fu Q, Si Y, Duan C, et al. (2019) Highly Carboxylated, Cellular Structured, and Underwater Superelastic Nanofibrous Aerogels for Efficient Protein Separation. Adv Funct Mater 29:1–11. 10.1002/adfm.201808234
20. Shuang Wu S, Wei M, Wei W, et al. (2019) Electrochemical aptasensor for aflatoxin B1 based on smart host-guest recognition of β-cyclodextrin polymer. 10.1016/j.bios.2019.01.022
21. Zhu X, Kou F, Xu H, et al. (2018) Label-free ochratoxin A electrochemical aptasensor based on target-induced noncovalent assembly of peroxidase-like graphitic carbon nitride nanosheet. Sensors Actuators B Chem 270:263–269. 10.1016/J.SNB.2018.05.048
22. Nan M, Bi Y, Xue H, et al. (2019) Rapid Determination of Ochratoxin A in Grape and Its Commodities Based on a Label-Free Impedimetric Aptasensor Constructed by Layer-by-Layer Self-Assembly. Toxins (Basel) 11:71 10.3390/toxins11020071
23. Abnous K, Danesh NM, Alibolandi M, et al. (2017) Amperometric aptasensor for ochratoxin A based on the use of a gold electrode modified with aptamer, complementary DNA, SWCNTs and the redox marker Methylene Blue. Microchim Acta 184:1151–1159. 10.1007/s00604-017-2113-7
24. Wei M, Wang C, Xu E, et al. (2019) A simple and sensitive electrochemiluminescence aptasensor for determination of ochratoxin A based on a nicking endonuclease-powered DNA walking machine. Food Chem 282:141–146. 10.1016/J.FOODCHEM.2019.01.011 [PubMed: 30711098]
25. Wang Y, Ning G, Bi H, et al. (2018) A novel ratiometric electrochemical assay for ochratoxin A coupling Au nanoparticles decorated MoS2 nanosheets with aptamer. Electrochim Acta 285:120–127. 10.1016/J.ELECTACTA.2018.07.195
26. El-Khouly AS, Takahashi Y, Saafan AA, et al. (2011) Study of heavy metal ion absorbance by amidoxime group introduced to cellulose-graft-polyacrylonitrile. J Appl Polym Sci 120:866–873. 10.1002/app.33135

27. Martins NCT, Freire CSR, Neto CP, et al. (2013) Antibacterial paper based on composite coatings of nanofibrillated cellulose and ZnO. Colloids Surfaces A Physicochem Eng Asp 417:111–119. 10.1016/J.COLSURFA.2012.10.042
28. Mandal B, Das D, Rameshbabu AP, et al. (2016) A biodegradable, biocompatible transdermal device derived from carboxymethyl cellulose and multi-walled carbon nanotubes for sustained release of diclofenac sodium. RSC Adv 6:19605–19611. 10.1039/C6RA00260A
29. Derikvand F, Yin DT, Barrett R, Brumer H (2016) Cellulose-Based Biosensors for Esterase Detection. Anal Chem 88:2989–2993. 10.1021/acs.analchem.5b04661 [PubMed: 26892369]
30. Mao Y, Huang X, Xiong S, et al. (2016) Large-volume immunomagnetic separation combined with multiplex PCR assay for simultaneous detection of Listeria monocytogenes and Listeria ivanovii in lettuce. Food Control 59:601–608. 10.1016/j.foodcont.2015.06.048
31. Amaly N, Ma Y, El-Moghazy AY, Sun G (2020) Copper complex formed with pyridine rings grafted on cellulose nanofibrous membranes for highly efficient lysozyme adsorption. Sep Purif Technol 250:117086 10.1016/j.seppur.2020.117086
32. El-Moghazy AY, Huo J, Amaly N, et al. (2020) An Innovative Nanobody-Based Electrochemical Immunosensor Using Decorated Nylon Nanofibers for Point-of-Care Monitoring of Human Exposure to Pyrethroid Insecticides. ACS Appl Mater Interfaces 12:6159–6168. 10.1021/acsami.9b16193 [PubMed: 31927905]
33. El-Moghazy AY, Zhao C, Istamboulie G, et al. (2018) Ultrasensitive label-free electrochemical immunosensor based on PVA-co-PE nanofibrous membrane for the detection of chloramphenicol residues in milk. Biosens Bioelectron 117:838–844. 10.1016/j.bios.2018.07.025 [PubMed: 30096738]
34. Amaly N, El-Moghazy AY, Si Y, Sun G (2020) Functionalized nanofibrous nylon 6 membranes for efficient reusable and selective separation of laccase enzyme. Colloids Surfaces B Biointerfaces 194:. 10.1016/j.colsurfb.2020.111190
35. Song J, Birbach NL, Hinestroza JP (2012) Deposition of silver nanoparticles on cellulosic fibers via stabilization of carboxymethyl groups. Cellulose 19:411–424. 10.1007/s10570-011-9647-3
36. Deng L, Young RJ, Kinloch IA, et al. (2013) Supercapacitance from Cellulose and Carbon Nanotube Nanocomposite Fibers. ACS Appl Mater Interfaces 5:9983–9990. 10.1021/am403622v [PubMed: 24070254]
37. Deng L, Young RJ, Kinloch IA, et al. (2013) Carbon nanofibres produced from electrospun cellulose nanofibres. Carbon N Y 58:66–75. 10.1016/J.CARBON.2013.02.032
38. Cruz-Aguado JA, Penner G (2008) Determination of ochratoxin A with a DNA aptamer. J Agric Food Chem 56:10456–10461. 10.1021/jf801957h [PubMed: 18983163]
39. Liu H HY (2002) Ultrafine fibrous cellulose membranes from electrospinning of cellulose acetate. J Polym Sci—Polym Phys 40:2119–2129
40. El-Moghazy AY, Soliman EA, Ibrahim HZ, et al. (2016) Biosensor based on electrospun blended chitosan-poly (vinyl alcohol) nanofibrous enzymatically sensitized membranes for pirimiphos-methyl detection in olive oil. Talanta 155:258–264. 10.1016/j.talanta.2016.04.018 [PubMed: 27216682]
41. Amiri P (2014) Electrospinning of Poly (acrylonitrile-acrylic acid)/ β Cyclodextrin Nanofibers and Study of their Molecular Filtration Characteristics. 1:14–21
42. Pasternack RM, Rivillon Amy S, Chabal YJ (2008) Attachment of 3-(Aminopropyl)triethoxysilane on Silicon Oxide Surfaces: Dependence on Solution Temperature. Langmuir 24:12963–12971. 10.1021/la8024827 [PubMed: 18942864]
43. Tao FF, Bernasek SL (2012) Functionalization of Semiconductor Surfaces
44. Seitz O, Fernandes PG, Tian R, et al. (2011) Control and stability of self-assembled monolayers under biosensing conditions. J Mater Chem 21:4384 10.1039/c1jm10132c
45. Yılmaz Baran N, Baran T, Menteş A (2017) Fabrication and application of cellulose Schiff base supported Pd(II) catalyst for fast and simple synthesis of biaryls via Suzuki coupling reaction. Appl Catal A Gen 531:36–44. 10.1016/j.apcata.2016.12.005
46. Qi X, Yoon H, Lee S-H, et al. (2008) Surface-modified imogolite by 3-APS–OsO4 complex: Synthesis, characterization and its application in the dihydroxylation of olefins. J Ind Eng Chem 14:136–141. 10.1016/J.JIEC.2007.08.010

47. Randles EB BJ (1948) A cathode ray polarograph. Trans Faraday Soc 44:322–327. 10.1039/tf9484400322

48. Eckhard K, Shin H, Mizaikoff B, et al. (2007) Alternating current (AC) impedance imaging with combined atomic force scanning electrochemical microscopy (AFM-SECM). Electrochem commun 9:1311–1315. 10.1016/J.ELECOM.2007.01.027

49. Santaclara FJ, Pérez-Martín RI, Sotelo CG (2014) Developed of a method for the genetic identification of ling species (Genypterus spp.) in seafood products by FINS methodology. Food Chem 143:22–26. 10.1016/j.foodchem.2013.06.004 [PubMed: 24054207]

50. White RJ, Phares N, Lubin AA, et al. (2008) Optimization of electrochemical aptamer-based sensors via optimization of probe packing density and surface chemistry. Langmuir 24:10513–10518. 10.1021/la800801v [PubMed: 18690727]

51. Muthamizh S, Ribes À, Anusuyajanakiraman M, et al. (2017) Implementation of oligonucleotide-gated supports for the electrochemical detection of Ochratoxin A. Supramol Chem 29:776–783. 10.1080/10610278.2017.1390238

52. De Girolamo A, McKeague M, Miller JD, et al. (2011) Determination of ochratoxin A in wheat after clean-up through a DNA aptamer-based solid phase extraction column. Food Chem 127:1378–1384. 10.1016/j.foodchem.2011.01.107 [PubMed: 25214141]

53. Guo X, Wen F, Zheng N, et al. (2020) Aptamer-Based Biosensor for Detection of Mycotoxins. Front Chem 8:. 10.3389/fchem.2020.00195

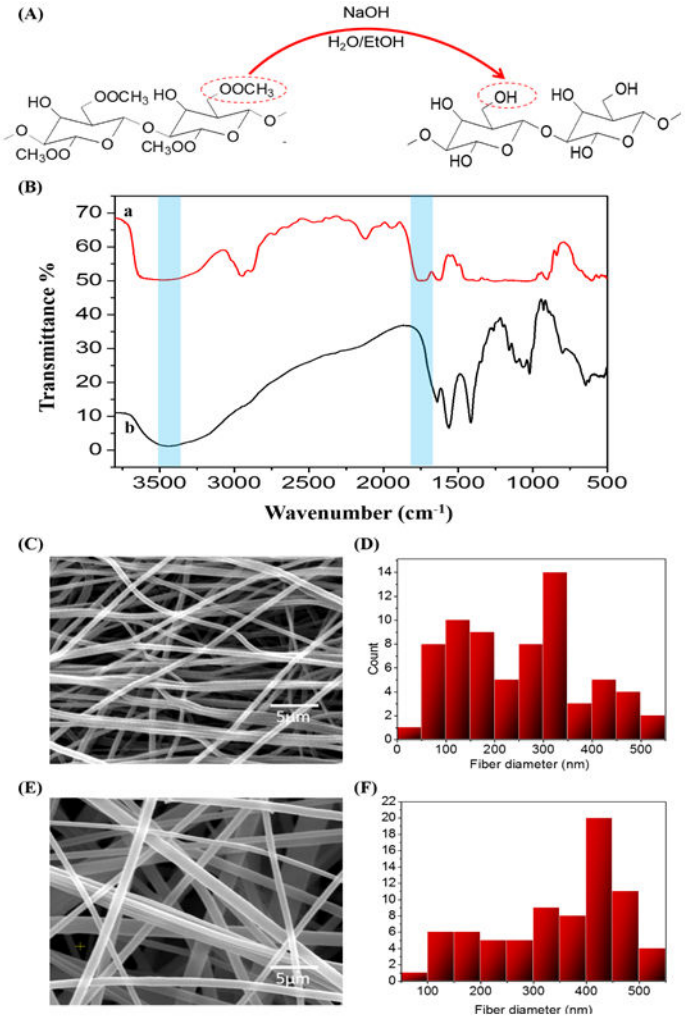

Fig. 1.:

(A) Scheme of deacetylation process of cellulose acetate. (B) FT-IR spectra of (a) cellulose acetate NFM, (b) regenerated Cel NFM. (C) SEM images and (D) diameter distribution of cellulose acetate NFM. (E) SEM images and (F) diameter distribution of Cel NFM.

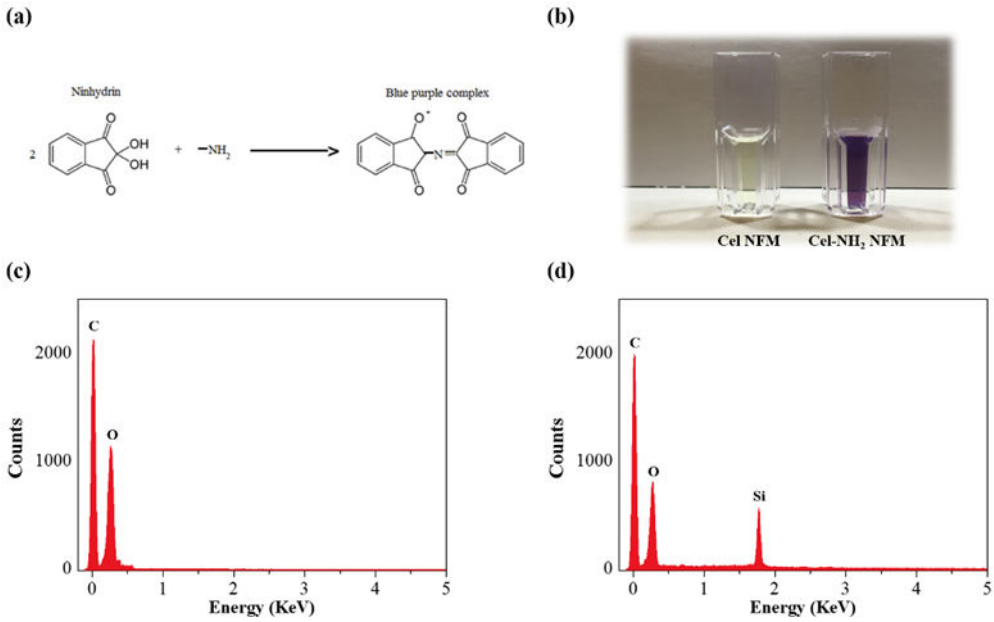

Fig. 2.

(a) Scheme of ninhydrin reaction with a primary amine group, (b) Ninhydrin color test for Cel NFM before and after modification with APTES, (c) EDX spectra of Cel NFM, (d) EDX spectra of Cel-NH_2 NFM.

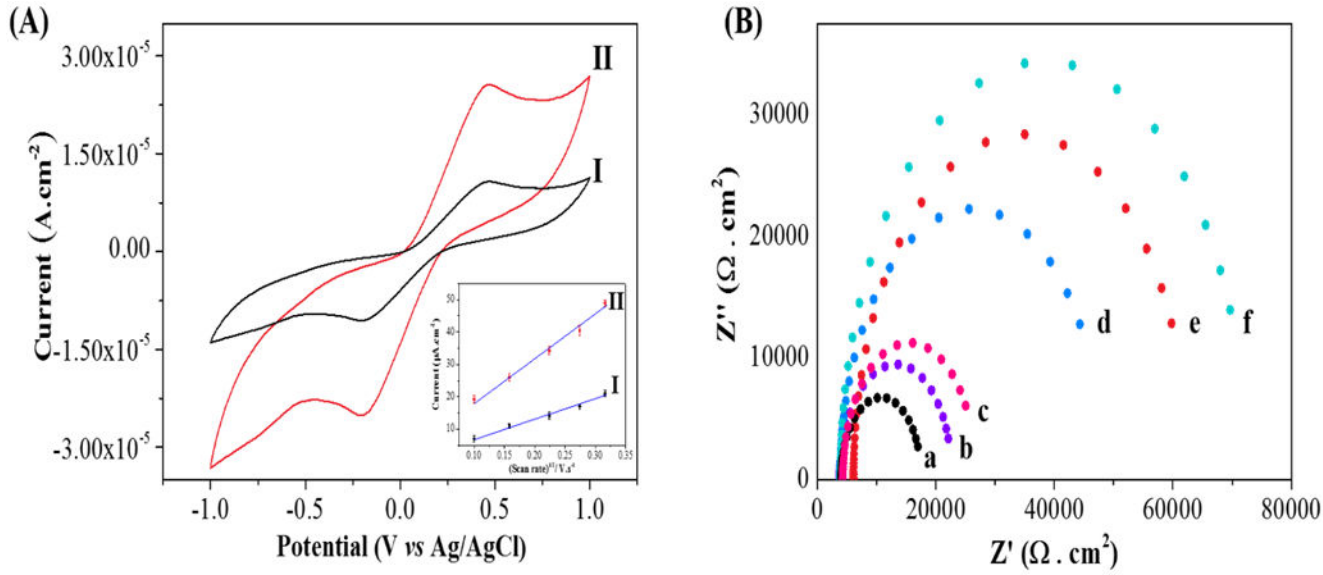

Fig. 3:

(A) Cyclic voltammograms of 2.5 mM $[Fe(CN)_6]^{3-/4-}$ at a scan rate of 25 mV s^{-1} for: (I) Cel CM/SPCE and (II) Cel NFM/SPCE. **(B)** Nyquist semicircle plots of EIS in 2.5 mM $[Fe(CN)6]^{4-/3-}$ of assembly steps of the OTA aptasensor: (a) unmodified SPCE, (b) Cel NFM/SPCE, (c) Cel-NH_2 NFM/SPCE, (d) Apt/Cel NFM/ SPCE, (e) EA/Apt/Cel NFM/ SPCE, and (f) OTA (0.5 ng mL^{-1}) /EA/Apt/Cel NFM/ SPCE.

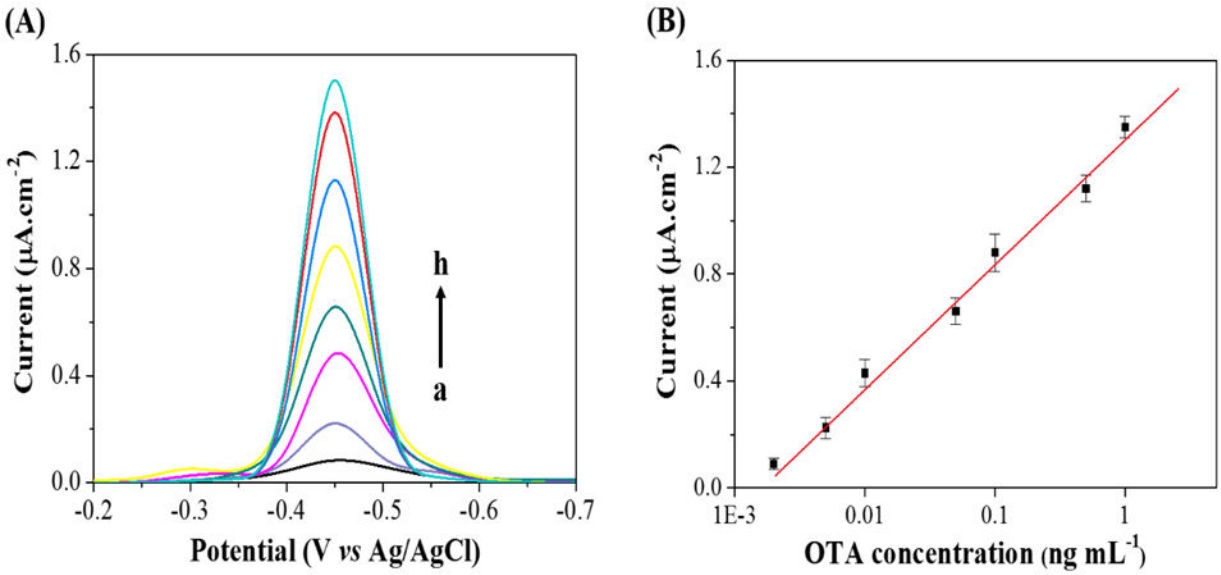

Fig. 4.

(A) DPVs responses of the fabricated aptasensor toward different OTA concentrations at applied potential range of −200 – −700 mV *vs* Ag/AgCl: (a) 0.002 ng mL^{-1}, (b) 0.005 ng mL^{-1}, (c) 0.01 ng mL^{-1}, (d) 0.05 ng mL^{-1}, (e) 0.1 ng mL^{-1}, (f) 0.5 ng mL^{-1}, (g) 1 ng mL^{-1}, (h) 2 ng mL^{-1}; (B) Calibration curve of the net response of aptasensor for OTA detection at different concentrations. *(n=3)*

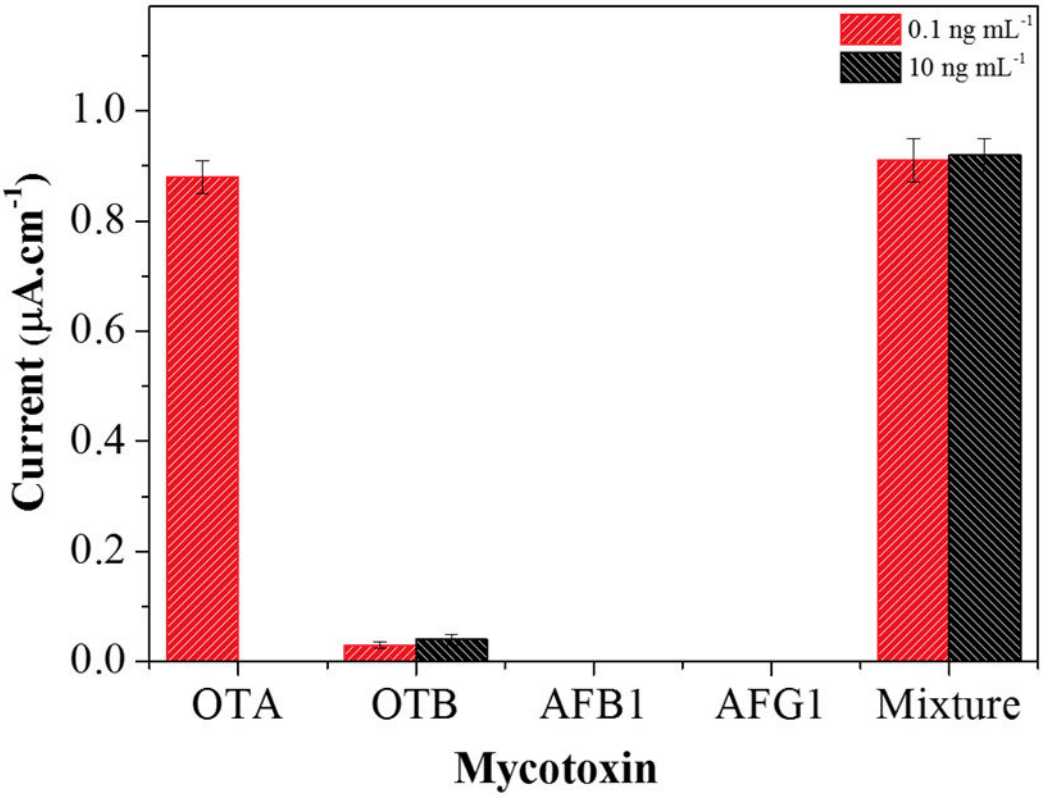

Fig. 5.
Specificity of the developed OTA aptasensor. (n=3)

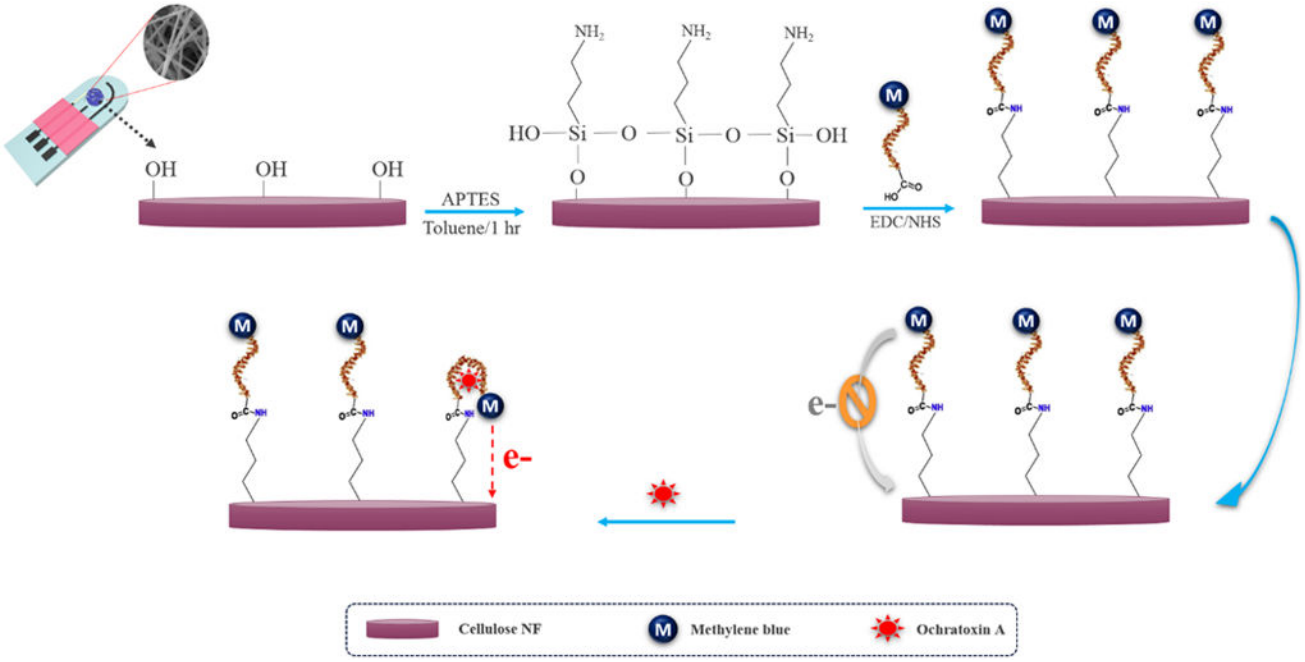

Scheme 1:
Fabrication process and sensing mechanism of OTA aptasensor

Table 1.

Comparison of the developed apatsensor with recently reported electrochemical OTA aptasensors:

	Electrochemical aptasensor	Range (ng mL^{-1})	LOD (pg mL^{-1})	Ref.
1	Apt-SWCNT-MB-AuE	0.07 - 12	21	[23]
2	Apt-mesoporous silica NPs-GCE	0.001 – 20	1.2	[51]
3	Apt/MoS_2-AuNPs-β-CD/AuE	0.04- 20	24.3	[25]
4	Apt/g-CNNS/AuE	0.08 - 200	29.6	[21]
5	Apt/AuNPs/CA/AuE	0.1 - 10.0	30	[22]
6	Apt/DNA/CdS QDs/GCE	0.02 - 2	4.9	[24]
7	Apt/Cel NFM/SPCE	0.002 - 2	0.81	This work

Apt – Aptamer; SWCNT – singled wall carbon nanotubes; MB – Methylene blue; AuE – Gold electrode; NPs – Nanoparticles; GCE – Glassy carbon electrode; AuNPs – Gold nanoparticles; β-CD – β-cyclodextrin; g-CNNS – graphite-like carbon nitride nanosheet; CdS QDs – Cadmium sulfide semiconductor quantum dots; Cel NFM – Cellulose nanofibrous membrane; SPCE – Screen-printed carbon electrode.